



Investigation of Gilbert damping of a tetragonally distorted ultrathin $\text{Fe}_{0.5}\text{Co}_{0.5}$ epitaxial film with high magnetic anisotropy

EP

Cite as: Appl. Phys. Lett. **113**, 232406 (2018); <https://doi.org/10.1063/1.5052721>

Submitted: 21 August 2018 . Accepted: 18 November 2018 . Published Online: 07 December 2018

R. Mandal , J. W. Jung, K. Masuda, Y. K. Takahashi, Y. Sakuraba, S. Kasai, Y. Miura, T. Ohkubo, and K. Hono 

COLLECTIONS

 This paper was selected as an Editor's Pick



View Online



Export Citation



CrossMark

ARTICLES YOU MAY BE INTERESTED IN

[Three-dimensional anisotropic thermal conductivity tensor of single crystalline \$\beta\text{-Ga}_2\text{O}_3\$](#)

Applied Physics Letters **113**, 232105 (2018); <https://doi.org/10.1063/1.5054573>

[Controlling shedding characteristics of condensate drops using electrowetting](#)

Applied Physics Letters **113**, 243703 (2018); <https://doi.org/10.1063/1.5064363>

[Perpendicular magnetic anisotropy in sputter-deposited Fe/MgO interfaces tuned by W buffer and Tb capping layers](#)

Applied Physics Letters **113**, 252401 (2018); <https://doi.org/10.1063/1.5038777>



Measure Ready
M91 FastHall™ Controller

A revolutionary new instrument
for complete Hall analysis

 Lake Shore
CRYOTRONICS



Investigation of Gilbert damping of a tetragonally distorted ultrathin Fe_{0.5}Co_{0.5} epitaxial film with high magnetic anisotropy

R. Mandal, J. W. Jung, K. Masuda, Y. K. Takahashi,^{a)} Y. Sakuraba, S. Kasai, Y. Miura, T. Ohkubo, and K. Hono

Research Center for Magnetic and Spintronic Materials, National Institute for Materials Science, 1-2-1 Sengen, Tsukuba 305-0047, Japan

(Received 21 August 2018; accepted 18 November 2018; published online 7 December 2018)

We have investigated the Gilbert damping, α , of a tetragonally distorted, perpendicular magnetic anisotropic (PMA) ultrathin Fe_{0.5}Co_{0.5} film grown on a Rh-buffered MgO(100) substrate fabricated by magnetron sputtering at room temperature by means of the time-resolved magneto-optical Kerr effect. We obtained the highest PMA value of 0.573 MJ/m³ ever reported for the Fe_{0.5}Co_{0.5}/Rh film. The PMA strongly depends on the lattice distortion which originates from the epitaxial growth in the large lattice misfit system of Fe_{0.5}Co_{0.5} and Rh. We have estimated an unusually high value of $\alpha = 0.041 \pm 0.002$ for a 1 nm thick Fe_{0.5}Co_{0.5} film. Based on the microstructural observation and the first-principles calculation, we conclude that the large α in the ultrathin Fe_{0.5}Co_{0.5} film comes from the minority-spin electron transition around the Fermi level mediated by the spin-orbit interaction, which is caused by the large lattice distortion. *Published by AIP Publishing.*

<https://doi.org/10.1063/1.5052721>

Ferromagnetic materials with large perpendicular magnetic anisotropy (PMA) have immense practical importance in the development of large capacity spin transfer torque magnetic random access memory (STT-MRAM)¹ that consisted of magnetic tunnel junctions (MTJs). Due to the demand to increase the capacity of STT-MRAM, the cell size was reduced by several tens of nanometers. To maintain the thermal stability and reduce the critical current density for spin-transfer torque (STT) switching, large PMA materials are strongly required² in MTJs for nonvolatile nature and high-speed operation. The origin of PMA is mainly based on two different reasons, such as the interfacial effect³ and the bulk-PMA originating from the strong spin-orbit coupling.⁴ Interfacially introduced PMA is reported in various material combinations with MgO^{3,5-12} and is introduced by the hybridization of orbitals between Fe in the ferromagnet and O in MgO.^{13,14} Using this interfacial PMA, a perpendicular MTJ was demonstrated.¹⁵ Bulk-PMA may also appear due to one more reason, which is lattice distortion.

Tetragonally distorted FeCo alloys have recently gained renewed attention as a promising PMA material due to their high magnetic anisotropy energy (K_u).¹⁶⁻¹⁸ In 2004, Burkert *et al.*¹⁶ first predicted that body-centered tetragonal (bct) Fe_{1-x}Co_x alloys could show a giant K_u of about 10 MJ/m³ at the Co concentration of $0.5 \leq x \leq 0.65$ and the tetragonal distortion (c/a) of $1.20 \leq c/a \leq 1.25$ based on the first-principles calculation. Afterwards, many experimental reports¹⁹⁻²¹ confirmed the large K_u in this particular alloy, but the values were appreciably smaller than the calculated value. It is also found that PMA is very sensitive to the induced tetragonal distortion. Therefore, the bct-FeCo alloy film should be epitaxially grown on suitable non-magnetic face-centered cubic (fcc) structures such as Pd ($c/a = 1.13$), Ir ($c/a = 1.18$) and

Rh ($c/a = 1.24$) substrates for achieving large K_u .¹⁷ Lao *et al.*²² reported the largest effective anisotropy K_u^{eff} ($= K_u - K_d$, where K_d is shape anisotropy) value of ~ 0.4 MJ/m³ with $c/a = 1.2$ for the Rh(001)-buffered Fe_{0.5}Co_{0.5} (1.5 nm) epitaxial film. There is still enough room to enhance the effective anisotropy by enhancing the c/a ratio. From the spintronic application point of view for PMA materials, the magnetic damping factor (α) is one of the important parameters to control the magnetization switching. In MTJ, the materials for a free layer should possess low α in order to reduce the critical current density for STT switching. On the other hand, high α is favorable for the reference layer material in order to maintain the unidirectional magnetization. In this study, we report the investigation of α in a tetragonally distorted Fe_{0.5}Co_{0.5} alloy thin film with high K_u^{eff} using a time-resolved magneto-optical Kerr effect (TR-MOKE) microscope. We obtained the largest K_u^{eff} value ever reported for ultrathin Fe_{0.5}Co_{0.5} films. In addition, a 1 nm thick Fe_{0.5}Co_{0.5} film shows unusually high α compared to a thicker film having in-plane anisotropy. Based on the microstructure observation and the first-principles calculation, we discuss the possible origins of the unusually high value of damping in ultrathin PMA films.

The thin films were deposited on a single crystalline MgO(100) substrate by an ultra-high vacuum magnetron sputtering system at a base pressure of 2×10^{-7} Pa. A 50 nm thick Rh underlayer was first deposited on top of the MgO(100) substrate at room temperature followed by post-annealing (T_a) at 573 K. Then, the Fe_{0.5}Co_{0.5} (t) layer was deposited at room temperature. The thickness t_{FeCo} varied from 1 to 10 nm. Finally, a 3 nm thick Rh protective layer was deposited at room temperature (T_d) on top of the Fe_{0.5}Co_{0.5} thin film (Fig. SI. 1) in order to avoid oxidation and degradation of the film quality with time and during the exposure of a high-power femtosecond laser beam at the time of TRMOKE experiments. To confirm the epitaxial

^{a)} Author to whom correspondence should be addressed: takahashi.yukiko@nims.go.jp

growth and the surface quality of the Rh underlayer and the $\text{Fe}_{0.5}\text{Co}_{0.5}$ layer, *in situ* reflection high-energy electron diffraction (RHEED) and atomic force microscopy (AFM) measurements were carried out (Fig. SI. 2). The crystalline structure was investigated using the conventional out-of-plane X-ray diffraction (XRD) with Cu $K\alpha$ radiation in the θ - 2θ geometry and using transmission electron microscopy (TEM). Magnetic hysteresis curves were measured at room temperature using a vibrating sample magnetometer (VSM) with in-plane and out-of-plane geometries. The torque magnetometry measurements²³ were carried out to calculate the effective uniaxial anisotropy for ultrathin $\text{Fe}_{0.5}\text{Co}_{0.5}$ films. The measurements were performed under the constant magnetic field by varying the direction of the magnetic field. The direction of magnetization at each constant value of the magnetic field angle helps to obtain the torque data which consist of the first- and second-orders of magnetic uniaxial anisotropy constant. The detailed explanation for this measurement with a schematic diagram of the experimental setup can be found in the [supplementary material](#) (SI. 3). The ultrafast magnetization dynamic measurements were carried out with an all-optical TR-MOKE microscope.²⁴ A high power mode-locked Yb:KGW laser (PHAROS, Light Conversion) with a wavelength of 1028 nm, a pulse width of 290 fs and a repetition rate of 10 kHz was used as a pump beam to excite the magnetization dynamics of the sample. The second harmonics ($\lambda = 515$ nm) of the fundamental laser beam was used as a probe to measure the magneto-optical Kerr rotation as a function of the time delay between the pump and probe beams with the help of the optical bridge detector and the lock-in-amplifier in a phase-sensitive manner. Both the pump and probe beams were focused onto the sample surface using a lens. The pump beam was modulated at 910 Hz using a mechanical chopper for the lock-in-detection. During the measurement, a variable external bias magnetic field ($\mu_0 H_b$) was applied at an angle of $\theta_H^{\text{TRMOKE}} = 60^\circ$ with respect to the perpendicular direction of the sample surface.

Figure 1 shows the change in the ratio of lattice parameter, the c/a ratio as a function of the film thickness of $\text{Fe}_{0.5}\text{Co}_{0.5}$, t_{FeCo} . The lattice parameter was calculated using Bragg's formula considering the $\text{Fe}_{0.5}\text{Co}_{0.5}(002)$ diffraction peak (marked by the blue arrow) in the XRD pattern shown in Fig. SI. 4. The c/a ratio was also calculated from the cross-sectional TEM image as shown as a red dot in Fig. 1(a) for the samples thinner than 2.5 nm. The c/a ratio is about 1.33 for $t_{\text{FeCo}} = 1$ nm and then reduces to 1.1 for $t_{\text{FeCo}} = 3$ nm. This rapid reduction of the c/a ratio with increasing film thickness follows the similar trend reported earlier.²⁵ The saturation magnetization as a function of film thickness is plotted in Fig. 1(c). Figures 1(d) and 1(e) compare the out-of-plane and in-plane magnetization curves of the $\text{Fe}_{0.5}\text{Co}_{0.5}$ thin films with $t_{\text{FeCo}} = 1$ and 3 nm, respectively. We found that the 1-nm-thick film shows PMA, whereas the films with $t_{\text{FeCo}} \geq 2.5$ nm show in-plane (IP) anisotropy. The effective magnetic anisotropy, K_u^{eff} calculated from the magnetization curves as well as the measured torque data are plotted as a function of t_{FeCo} , as shown in Fig. 1(b). PMA is realized in films with $t_{\text{FeCo}} \leq 2.0$ nm and decreases with t_{FeCo} . The $t_{\text{FeCo}} = 1.5$ nm film shows the highest K_u^{eff} value of 0.573 MJ/m^3 in the

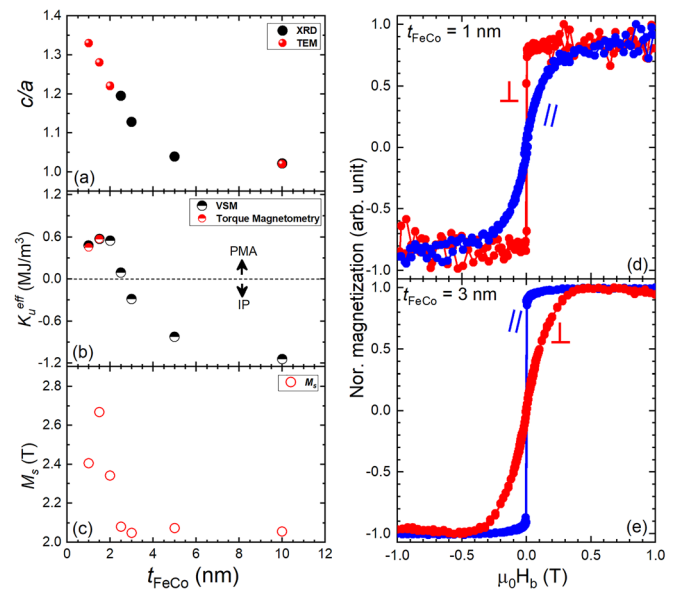


FIG. 1. (a) The lattice parameter, the c/a ratio, (b) the effective magnetic anisotropy, K_u^{eff} and (c) the saturation magnetization for $\text{Fe}_{0.5}\text{Co}_{0.5}$ film as a function t_{FeCo} and magnetization curves of the $\text{Fe}_{0.5}\text{Co}_{0.5}$ thin film of thickness $t_{\text{FeCo}} = 1$ nm (d) and 3 nm (e). Red and blue symbols correspond to the out-of-plane and in-plane directions.

tetragonally distorted $\text{Fe}_{0.5}\text{Co}_{0.5}$ thin film till date. For $t_{\text{FeCo}} = 1$ and 1.5 nm, both the torque data and magnetization data matched well with each other.

Figure 2(a) shows the typical time-resolved Kerr rotation spectra recorded with a TR-MOKE microscope for a $t_{\text{FeCo}} = 1.5$ nm thin film in the presence of $\mu_0 H_b$ ranging from 0.58 T to 1.85 T. The details of this Kerr signal are explained in SI. 5. The $t_{\text{FeCo}} = 1.5$ nm thin film shows a single uniform resonance frequency (f_r) mode. In order to extract f_r and the relaxation time (τ), the TR-MOKE signal is fitted with a well-defined phenomenological fitting function

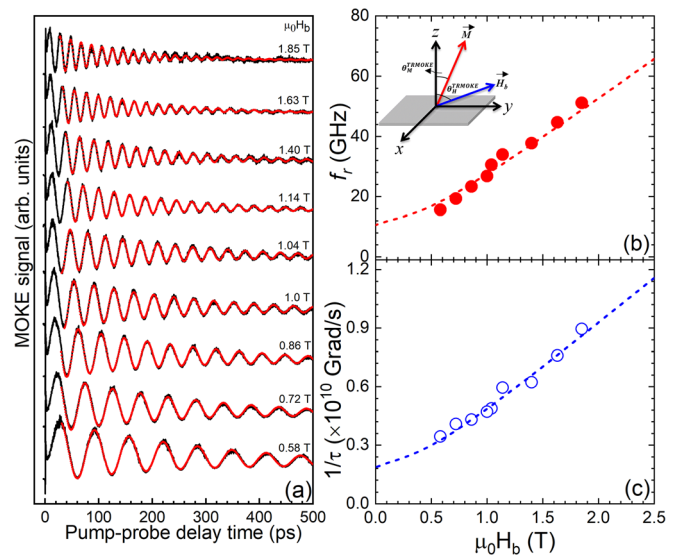


FIG. 2. (a) Typical time-resolved Kerr signal for $t_{\text{FeCo}} = 1.5$ nm thick $\text{Fe}_{0.5}\text{Co}_{0.5}$ film under an external magnetic bias field with different strengths. The red dotted curves are the fitted curve of the experimental data to Eq. (1). The inset in (b) shows the schematics of the experimental geometry. (b) The resonance precession frequency f_r and (c) the inverse relaxation time $1/\tau$ as a function of external bias magnetic field strength. The broken curves are fits using the linearized LLG equation.

$$\theta_k(t) = Ae^{-t/\tau} + B\sin(2\pi f_r t + \varphi)e^{(-t/\tau)} + C, \quad (1)$$

where A , B , and C are the demagnetization magnitude, the oscillatory motion amplitude, and an offset, respectively. f_r , t_1 , τ , and φ are the resonance frequency, the recovery rate, the relaxation time, and the initial phase, respectively. Figures 2(b) and 2(c) show the $\mu_0 H_b$ dependence of f_r and $1/\tau$ in the case of $t_{\text{FeCo}} = 1.5$ nm film. Using the linearized LLG equation, f_r , $1/\tau$ and their field components H_1^{TRMOKE} , H_2^{TRMOKE} are derived²⁶ such as: $f_r = \frac{\gamma}{2\pi} \sqrt{H_1^{\text{TRMOKE}} H_2^{\text{TRMOKE}}}$; $\frac{1}{\tau} = \frac{1}{2} \alpha \gamma (H_1^{\text{TRMOKE}} + H_2^{\text{TRMOKE}})$; $H_1^{\text{TRMOKE}} = H_b \cos(\theta_M^{\text{TRMOKE}} - \theta_H^{\text{TRMOKE}}) + H_k^{\text{eff}} \cos^2 \theta_M^{\text{TRMOKE}}$ and $H_2^{\text{TRMOKE}} = H_b \cos(\theta_M^{\text{TRMOKE}} + \theta_H^{\text{TRMOKE}}) + H_k^{\text{eff}} \cos^2 \theta_M^{\text{TRMOKE}}$. Here, γ ($= \frac{g\mu_B}{\hbar}$), α , H_k^{eff} , θ_M^{TRMOKE} , and θ_H^{TRMOKE} are the gyromagnetic ratio, the Gilbert damping constant, the effective anisotropy field and the equilibrium angles of magnetization and the bias magnetic field with respect to the z direction, respectively. θ_M^{TRMOKE} can be derived from the equation: $\sin 2\theta_M^{\text{TRMOKE}} = \frac{2H_b}{H_k^{\text{eff}}} \sin(\theta_M^{\text{TRMOKE}} - \theta_H^{\text{TRMOKE}})$. By considering $g = 2$, we evaluated the value of $H_k^{\text{eff}} = 0.4$ T from the LLG fitting. The evaluated H_k^{eff} is similar to the saturation field that was obtained from the magnetization curve. We found that both experimental f_r and $1/\tau$ qualitatively match with the data calculated using the LLG equation as shown in Figs. 2(b) and 2(c). Figure 3 shows the change in α as a function of the inverse of the film thickness, $1/t_{\text{FeCo}}$. We found that the values of α consistently increased with the increase in $1/t_{\text{FeCo}}$, which corresponds to the decrease in the film thickness. In particular, α linearly increases from 0.029 ± 0.002 for $t_{\text{FeCo}} = 1.5$ nm to 0.041 ± 0.002 for $t_{\text{FeCo}} = 1$ nm as a function of the inverse of the film thickness. In order to understand the possible origins of large α , we carried out scanning transmission electron microscope (STEM) analyses for $t_{\text{FeCo}} = 1$ and 10 nm. Figure 4 shows the cross-sectional high-angle annular dark field (HAADF)-STEM images for the $t_{\text{FeCo}} = 1$ and 10 nm films, respectively. We observe that the lattice parameter along the c -axis is elongated (refer to the enlarged image of the $\text{Fe}_{0.5}\text{Co}_{0.5}$ layer in the inset) compared to the a -axis. But, for $t_{\text{FeCo}} = 10$ nm, both lattice

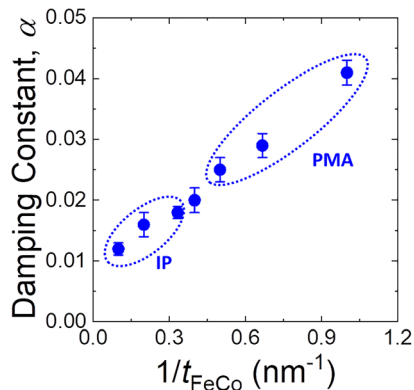


FIG. 3. The Gilbert damping constant α plotted as a function of the inverse of the $\text{Fe}_{0.5}\text{Co}_{0.5}$ thickness, $1/t_{\text{FeCo}}$. The blue symbols correspond to the damping constant and the blue dotted parabola defines the two different class of magnetization i.e., PMA and IP.

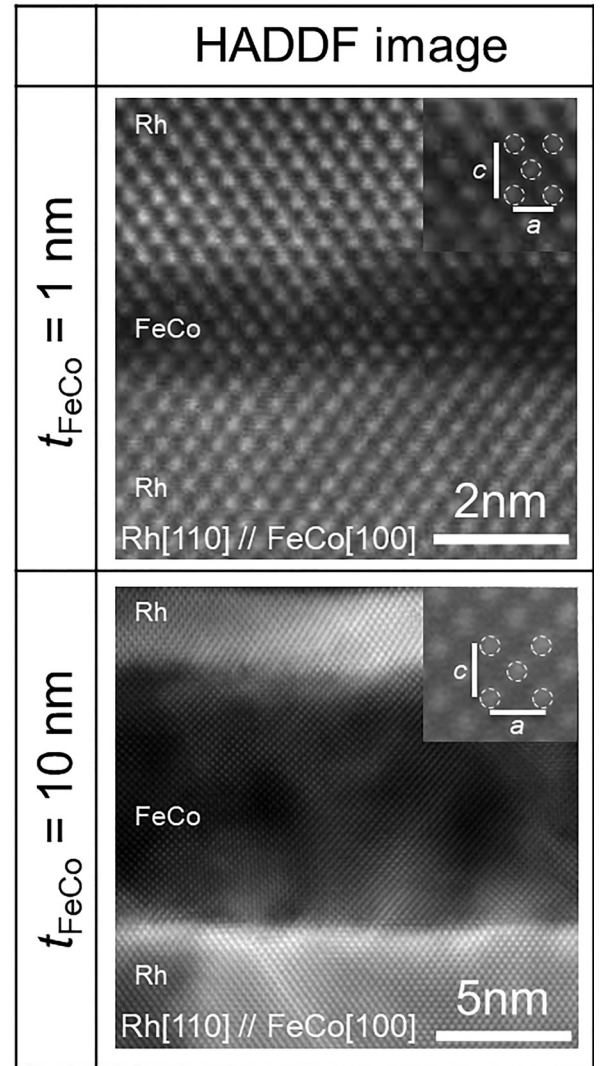


FIG. 4. Cross-sectional HAADF-STEM images (magnified image of $\text{Fe}_{0.5}\text{Co}_{0.5}$ layer is in the inset; the c -axis and a -axis of lattice is shown by the line) for $t_{\text{FeCo}} = 1$ and 10 nm $\text{Fe}_{0.5}\text{Co}_{0.5}$ thin film.

parameters c and a are comparable to each other. The microstructural observation implies that the increase in the c/a ratio, i.e., the tetragonal distortion may make an important contribution to the enhancement of α . In search for the origin of the large α value, we performed first-principles density-functional calculations based on the microstructural analyses.

Recent studies^{26–28} have analyzed damping constants α of several ferromagnets on the basis of Kambersky's torque-correlation model²⁹ by using the first-principles calculation. In this work, we adopted the same method and directly calculated the damping constants α of cubic (bcc) and tetragonally distorted (bct) $\text{Fe}_{0.5}\text{Co}_{0.5}$. Details of the calculation are given in Ref. 26. On the basis of STEM observations, we fixed the lattice parameter to $a = 2.842$ Å and $a = 2.726$ Å ($c/a = 1.33$) for bcc and bct $\text{Fe}_{0.5}\text{Co}_{0.5}$, respectively. In these calculations, we assumed the B2-ordered structure in $\text{Fe}_{0.5}\text{Co}_{0.5}$, because the electronic structure around the Fermi level is similar between the B2-ordered and fully disordered $\text{Fe}_{0.5}\text{Co}_{0.5}$ as shown in Fig. 5.

We obtained $\alpha = 0.0066$ and 0.0178 for bcc and bct $\text{Fe}_{0.5}\text{Co}_{0.5}$, respectively, which is qualitatively consistent

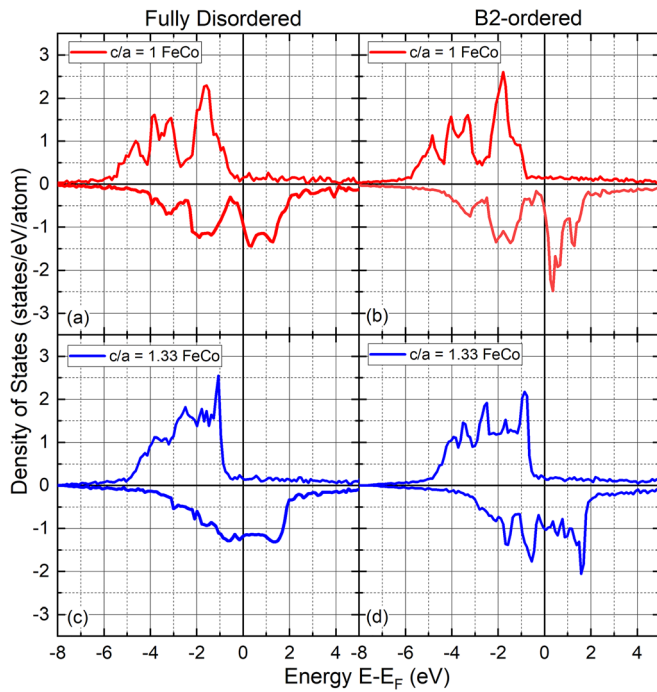


FIG. 5. Density of states (DOS) of $\text{Fe}_{0.5}\text{Co}_{0.5}$ for (a) fully disordered bcc case, (b) B2-ordered bcc case, (c) fully disordered bct case, and (d) B2-ordered bct case.

with our experimental observations mentioned above. To understand these theoretical results, we also analyzed the density of states (DOS) of bcc and bct $\text{Fe}_{0.5}\text{Co}_{0.5}$ by using the Akai-KKR code.³⁰ Figures 5(a) and 5(c) [5(b) and 5(d)] show the DOSs of the fully disordered (B2-ordered) $\text{Fe}_{0.5}\text{Co}_{0.5}$ with bcc and bct structures, respectively. We see that the DOSs around the Fermi level (E_F) in the B2-ordered $\text{Fe}_{0.5}\text{Co}_{0.5}$ are similar to those in the fully disordered $\text{Fe}_{0.5}\text{Co}_{0.5}$, justifying our assumption in the calculation of α . We also find that when the lattice is distorted from bcc to bct structure, the pseudogap around E_F in the minority-spin DOS closes, leading to the increase in the occupied minority-spin states just below E_F [see Figs. 5(c) and 5(d)]. In Kambersky's torque-correlation model,²⁹ the expression of the damping constant α includes the transition matrix element, which has contributions from spin-conserving and spin-flip electron transitions around E_F due to the spin-orbit interaction.³¹ The increase in the occupied minority-spin states just below E_F [Figs. 5(c) and 5(d)] enhances the spin-conserving electron transition between unoccupied and occupied minority-spin states around E_F , which would be the main origin of enhancement of the damping constant in $\text{Fe}_{0.5}\text{Co}_{0.5}$ due to the tetragonal distortion. The spin pumping effect and the inhomogeneous anisotropy distribution could be considered as other possible origins of the large α value. The inhomogeneous anisotropy distribution causes a change in the relaxation time; however, Fig. 2(c) shows that the relaxation time increases monotonically with the external bias field. So, we can rule out the possibility of the inhomogeneous anisotropy distribution. The possibility of the spin pumping effect at the interface of Rh and the $\text{Fe}_{0.5}\text{Co}_{0.5}$ layer depends on the spin-Hall angle of Rh. Rh is known to have a low spin-Hall angle^{32,33} like Ru³⁴ and Pd³⁵ following the similar trend of spin-Hall conductivity.³⁶ Earlier work also

reported that the spin-pumping effect is relatively small due to the small spin-Hall angle of Ru in the Ru/CoFeAl interface. We also calculated the spin-mixing conductance of the $\text{Fe}_{0.5}\text{Co}_{0.5}$ film as a function of film thickness (described in supplementary material 6) and found that the value is almost constant from ultrathin to thicker $\text{Fe}_{0.5}\text{Co}_{0.5}$ film. So, in the case of Rh/ $\text{Fe}_{0.5}\text{Co}_{0.5}$ interface, we can also expect relatively small spin-pumping effect contribution. Therefore, we conclude that the lattice distortion plays one of the significant roles in enhancing the Gilbert damping of $\text{Fe}_{0.5}\text{Co}_{0.5}$.

In conclusion, we investigated the Gilbert damping coefficient, α , of a tetragonally distorted ultrathin epitaxial $\text{Fe}_{0.5}\text{Co}_{0.5}$ film grown on the Rh underlayer using a TR-MOKE microscope. The highest effective anisotropy, K_u^{eff} , value of 0.573 MJ/m³ was observed for the 1.5 nm thick $\text{Fe}_{0.5}\text{Co}_{0.5}$ film. We observed the increase in α for the ultrathin $\text{Fe}_{0.5}\text{Co}_{0.5}$ film, and it reaches 0.041 ± 0.002 for the 1 nm thick film. The enhancement of α was explained qualitatively by the microstructural analyses and the first-principle calculations. From TEM analyses, we found that the lattice distortion increases from 1.02 to 1.33 with a decrease in t_{FeCo} . From the first-principles calculation, we found that the minority-spin electron transition due to the spin-orbit interaction enhances by introducing the tetragonal distortion. Therefore, the tetragonal distortion plays a notable role in the origin of large α for the ultrathin $\text{Fe}_{0.5}\text{Co}_{0.5}$ film. In the application point of view, the tetragonally distorted $\text{Fe}_{0.5}\text{Co}_{0.5}$ film with high PMA and α is suitable as a reference layer for MTJ in STT-MRAM, but not for the free-layer electrode as its damping is too high for low current STT switching.

See supplementary material for the schematic view of the film stack (supplementary material 1), RHEED and AFM images of $\text{Fe}_{0.5}\text{Co}_{0.5}$ and Rh layer. (supplementary material 2), the experimental details of torque magnetometry (supplementary material 3), the XRD patterns of various thicknesses of $\text{Fe}_{0.5}\text{Co}_{0.5}$ thin films (supplementary material 4), the typical time-resolved Kerr signal of 1.5 nm thick $\text{Fe}_{0.5}\text{Co}_{0.5}$ thin film (supplementary material 5) and the calculation of spin mixing conductance of $\text{Fe}_{0.5}\text{Co}_{0.5}$ thin films (supplementary material 6).

This work was supported by JSPS KAKENHI Grant Nos. 18H03787 and 17H06152 and the ImPACT Program of Council for Science, Technology and Innovation, Japan. We also thank Dr. I. Suzuki for technical assistance during the X-ray diffraction measurements and H. Tajiri and L. S. R. Kumara for their help in analysing the crystal structure of $\text{Fe}_{0.5}\text{Co}_{0.5}$ in this work.

¹D. Apalkov, B. Dieny, and J. M. Slaughter, *Proc. IEEE* **104**(10), 1796–1830 (2016).

²B. Dieny, B. R. Goldfarb, and K. J. Lee, *Introduction to Magnetic Random-access Memory* (Wiley, Hoboken, NJ, 2016).

³S. Ikeda, K. Miura, H. Yamamoto, K. Mizunuma, H. D. Gan, M. Endo, S. Kanai, J. Hayakawa, F. Matsukura, and H. Ohno, *Nat. Mater.* **9**, 721 (2010).

⁴D. Weller, A. Moser, L. Folks, M. E. Best, L. Wen, M. F. Toney, M. Schwickert, J. U. Thiele, and M. F. Doerner, *IEEE Trans. Magn.* **36**, 10–15 (2000).

- ⁵L. E. Nistor, B. Rodmacq, S. Auffret, and B. Dieny, *Appl. Phys. Lett.* **94**, 012512 (2009).
- ⁶C. H. Lambert, A. Rajanikanth, T. Hauet, S. Mangin, E. E. Fullerton, and S. Andrieu, *Appl. Phys. Lett.* **102**, 122410 (2013).
- ⁷T. Maruyama, Y. Shiota, T. Nozaki, K. Ohta, N. Toda, M. Mizuguchi, A. A. Tulapurkar, T. Shinjo, M. Shiraishi, S. Mizukami, Y. Ando, and Y. Suzuki, *Nat. Nanotechnol.* **4**, 158 (2009).
- ⁸S. Kanai, Y. Nakatani, M. Yamanouchi, S. Ikeda, H. Sato, F. Matsukura, and H. Ohno, *Appl. Phys. Lett.* **104**, 212406 (2014).
- ⁹Z. Wen, H. Sukegawa, S. Mitani, and K. Inomata, *Appl. Phys. Lett.* **98**, 242507 (2011).
- ¹⁰Y. Takamura, T. Suzuki, Y. Fujino, and S. Nakagawa, *J. Appl. Phys.* **115**, 17C732 (2014).
- ¹¹T. Kamada, T. Kubota, S. Takahashi, Y. Sonobe, and K. Takanashi, *IEEE Trans. Magn.* **50**, 1–4 (2014).
- ¹²K. Nakamura, T. Akiyama, T. Ito, M. Weinert, and A. J. Freeman, *Phys. Rev. B* **81**, 220409 (2010).
- ¹³H. X. Yang, M. Chshiev, B. Dieny, J. H. Lee, A. Manchon, and K. H. Shin, *Phys. Rev. B* **84**, 054401 (2011).
- ¹⁴J. W. Koo, S. Mitani, T. T. Sasaki, H. Sukegawa, Z. C. Wen, T. Ohkubo, T. Niizeki, K. Inomata, and K. Hono, *Appl. Phys. Lett.* **103**, 192401 (2013).
- ¹⁵K. Woojin, J. H. Jeong, Y. Kim, W. C. Lim, J. H. Kim, J. H. Park, H. J. Shin, Y. S. Park, K. S. Kim, S. H. Park, Y. J. Lee, K. W. Kim, H. J. Kwon, H. L. Park, H. S. Ahn, S. C. Oh, J. E. Lee, S. O. Park, S. Choi, H. K. Kang, and C. Chung, in paper presented at the 2011 International Electron Devices Meeting, 2011.
- ¹⁶T. Burkert, L. Nordström, O. Eriksson, and O. Heinonen, *Phys. Rev. Lett.* **93**, 027203 (2004).
- ¹⁷F. Yildiz, M. Przybylski, X. D. Ma, and J. Kirschner, *Phys. Rev. B* **80**, 064415 (2009).
- ¹⁸P. Warnicke, G. Andersson, M. Björck, J. Ferré, and P. Nordblad, *J. Phys.: Condens. Matter* **19**, 226218 (2007).
- ¹⁹G. Andersson, T. Burkert, P. Warnicke, M. Björck, B. Sanyal, C. Chacon, C. Zlotea, L. Nordström, P. Nordblad, and O. Eriksson, *Phys. Rev. Lett.* **96**, 037205 (2006).
- ²⁰F. Luo, X. L. Fu, A. Winkelmann, and M. Przybylski, *Appl. Phys. Lett.* **91**, 262512 (2007).
- ²¹F. Yildiz, F. Luo, C. Tieg, R. M. Abrudan, X. L. Fu, A. Winkelmann, M. Przybylski, and J. Kirschner, *Phys. Rev. Lett.* **100**, 037205 (2008).
- ²²B. Lao, J. W. Jung, and M. Sahaishi, *IEEE Trans. Magn.* **50**, 1–4 (2014).
- ²³T. Ono, N. Kikuchi, S. Okamoto, O. Kitakami, and T. Shimatsu, *Appl. Phys. Express* **11**, 033002 (2018).
- ²⁴Q. Xiang, R. Mandal, H. Sukegawa, Y. K. Takahashi, and S. Mitani, *Appl. Phys. Express* **11**, 063008 (2018).
- ²⁵H. Oomiya, B. Wang, S. Yoshida, T. Kataguchi, K. Takahashi, S. Kanatani, L. Zhang, L. Liu, T. Hasegawa, K. Hayasaka, S. Saito, N. Inami, T. Ueno, K. Ono, and S. Ishio, *J. Phys. D: Appl. Phys.* **48**, 475003 (2015).
- ²⁶Y. K. Takahashi, Y. Miura, R. Choi, T. Ohkubo, Z. C. Wen, K. Ishioka, R. Mandal, R. Medapalli, H. Sukegawa, S. Mitani, E. E. Fullerton, and K. Hono, *Appl. Phys. Lett.* **110**, 252409 (2017).
- ²⁷K. Gilmore, Y. U. Idzerda, and M. D. Stiles, *Phys. Rev. Lett.* **99**, 027204 (2007).
- ²⁸A. Sakuma, *J. Phys. D: Appl. Phys.* **48**, 164011 (2015).
- ²⁹V. Kamberský, *Czech. J. Phys. B* **26**, 1366–1383 (1976).
- ³⁰See <http://kkriissp.u-tokyo.ac.jp/jp/> for detailed information about the Akai-KKR code.
- ³¹C. Liu, C. K. A. Mewes, M. Chshiev, T. Mewes, and W. H. Butler, *Appl. Phys. Lett.* **95**, 022509 (2009).
- ³²H. Kontani, T. Tanaka, D. S. Hirashima, K. Yamada, and J. Inoue, *Phys. Rev. Lett.* **102**, 016601 (2009).
- ³³T. Shang, Q. F. Zhan, L. Ma, H. L. Yang, Z. H. Zuo, Y. L. Xie, H. H. Li, L. P. Liu, B. M. Wang, Y. H. Wu, S. Zhang, and R.-W. Li, *Sci. Rep.* **5**, 17734 (2015).
- ³⁴Z. Wen, J. Kim, H. Sukegawa, M. Hayashi, and S. Mitani, *AIP Adv.* **6**, 056307 (2016).
- ³⁵X. D. Tao, Z. Feng, B. F. Miao, L. Sun, B. You, D. Wu, J. Du, W. Zhang, and H. F. Ding, *J. Appl. Phys.* **115**, 17C504 (2014).
- ³⁶T. Tanaka, H. Kontani, M. Naito, T. Naito, D. S. Hirashima, K. Yamada, and J. Inoue, *Phys. Rev. B* **77**, 165117 (2008).